Sustainable γ-cyclodextrin frameworks containing ultra-fine silver nanoparticles with enhanced antimicrobial efficacy

Hessah Alotaibi[1,4†], Etelka Chung[3†], Se Hun Chung[1], Guogang Ren[3*] Vikramjeet Singh[1,2*] and Jie Huang[1*]

[1]Department of Mechanical Engineering, University College London, Torrington Place, London WC1E 7JE, UK

[2]Nanoengineered Systems Laboratory, UCL Mechanical Engineering, University College London, London, WC1E 7JE, UK

[3]School of Engineering & Computer Science, University of Hertfordshire, Hatfield, AL10 9AB, UK

[4]Department of Biomedical Engineering, King Faisal University, Hofuf, 31982, Saudi Arabia

† These authors contribute equally

Corresponding authors email: g.g.ren@herts.ac.uk, singh.simm@outlook.com, jie.huang@ucl.ac.uk

Abstract

Cyclodextrin metal-organic frameworks (CD-MOF) are a class of biocompatible MOFs with a great potential in drug delivery applications. Original CD-MOF crystals are fragile and large (0.2-1 mm), which are less useful in pharmaceutical applications. Cetyltrimethylammonium bromide and long chain poly(ethylene) glycol, used in size modulation to produce nanosized CD-MOF can compromise the biocompatibility, and physiochemical properties of CD-MOF as their complete removal from frameworks is difficult. To avoid the use of above-mentioned modulators, herein, we demonstrate the synthesis of nanosized CD-MOF using triethylamine (TEA) as a modulator to reduce their size to ~254 nm. The MOF characteristics such as crystal and chemical structure remain unaffected and the surface area of CD-MOF synthesised with TEA is measured 1075.5 m^2/g, almost 50% higher than those of synthesised using bulky modulators. The improved CD-MOF architecture utilised for the *in-situ* synthesis of silver nanoparticles resulted in enhanced antimicrobial efficacy tested against *Staphylococcus aureus* and *Escherichia coli* bacteria and *Candida albicans* fungus. And minimum inhibitory concentration (MIC) is recorded in the range of 31-15 µg/mL. Overall, the structural improvement in CD-MOF supported with thorough comparative investigations and enhanced antimicrobial efficacy could be very helpful in further establishing them in biomedicine field.

Keywords
Cyclodextrin metal-organic frameworks, triethylamine, antimicrobial, silver nanoparticles, modulators,

1. Introduction

Microbial-induced infectious diseases are a serious threat to human life and world economy causing millions of deaths each year world-wide (Larsson and Flach, 2022). After the discovery of Penicillin in 1928, the first antibiotic, thousands of drugs have been developed and antibiotics remain an indispensable approach to fight these dangerous micro-organisms including bacteria, and fungi (Wenzel, 2020). However, microbes, especially bacteria started developing resistance against these antibiotics over the time due to misuse and overuse of these drugs, overgrowing population, poor sanitation and inappropriate sewage system (Fouz et al., 2020; Larson, 2007). Research has been ramped up to find alternatives to save human life and of all the antimicrobial materials such as metal-ion materials, organic materials, photocatalytic materials and natural compounds, nanoparticles-based approach has attracted great attention due to its high efficacy (Staroń and Długosz, 2021). In particular, silver nanoparticles (AgNPs) possess a broad spectrum of antimicrobial activities due to their ability to penetrate microbial cell walls and interrupt cell deoxyribonucleic acid replication through release of sliver ions (Dakal et al., 2016). Apart from studying the mechanism of action, the effect of size, shape, charge, coating/capping, agglomeration and purity of AgNPs on the antimicrobial activity have been exploited extensively (Hong et al., 2016; Skandalis et al., 2017). The size of AgNPs was found to have a significant impact - smaller AgNPs exhibit higher antibacterial activity compared to the larger nanoparticles. It is concluded that AgNPs with size smaller than the 100 nm interacts well and could penetrate the cell wall more efficiently to reach the cytoplasm (site of action) (Agnihotri et al., 2014). In addition to all of the excellent properties, one of the major drawbacks which is preventing AgNPs to be used as commercial antimicrobial materials is their poor underwater stability (Fernando and Zhou, 2019). Water-based nanoparticles suspensions tend to aggregate, resulting into loss of their antimicrobial functionality. The use of polymers, proteins and other stabilizing agents (surfactants) to prevent their aggregation is either inefficient or involves hazardous chemicals which compromise the biocompatibility of the formulation (Akter et al., 2018; Andrieux-Ledier et al., 2013). AgNPs have been incorporated into polymer matrix, zeolites or metal-organic frameworks (MOF) for the stability enhancement (Li et al., 2022; Rifai et al., 2006; Torres-Flores et al., 2021). MOF, a new class of porous materials have been exploited for their use in improving the stability of drugs and nanoparticles (Cao et al., 2021; Cure et al., 2019; Luzuriaga et al., 2019) in addition to other applications such as gas storage, imaging, sensing, catalysis due to their well-defined porosity and tunable size and structure (Lawson et al., 2021). Especially, cyclodextrin based MOF (CD-MOF) is the centre of attention in drug delivery research field due to: i)

facile synthesis from edible components such as starch derived cyclic oligosaccharides (cyclodextrins), alkali metals (potassium hydroxide) and alcohols (ethanol), ii) dual cavities from cyclodextrin molecules (0.7 nm) and framework architecture (1.7 nm) and iii) exceptional capability of cyclodextrins to form inclusion complex with the wide variety of molecules (He et al., 2019; Liu et al., 2016). Specifically, in healthcare, CD-MOF have been exploited for targeted drug delivery of anti-cancer drugs, dry powder inhalation, solubility enhancer and antibacterial materials (Huang et al., 2022; Shakya et al., 2019; Zhang et al., 2018). Several structure improvement studies have been also conducted to overcome the moisture sensitive nature of CD-MOF such as by grafting cholesterol molecules on the surface, incorporating fullerene (C60) into their cavities and forming hydrogel by directly cross-linking cyclodextrin units with ethylene glycol and diphenyl carbonate (Li et al., 2016; Singh et al., 2017a; Singh et al., 2017b).

In an interesting finding, nanocavities of CD-MOF have been utilized as nanoreactors for the synthesis of ultrafine AgNPs with a diameter of ~2-5 nm and their applicability as electric conductors has been demonstrated (Wei et al., 2012). Shakya et al., have shown the use of these AgNPs loaded CD-MOF as potential anti-bacterial material and the aqueous stability of nanoparticles was enhanced significantly after incorporation into the nanoporous framework (Shakya et al., 2019). The size of as synthesized CD-MOF is in the range of millimetre (200 µm to 1 mm) and not suitable for drug delivery applications due to their highly fragile and full-of-cracks architecture. Size modulation using acids, bases or surfactants is a popular method to improve the synthesis reproducibility and control the shape and size of MOF (Wang et al., 2022; Zahn et al., 2014). In all CD-MOF work mentioned above, their size was reduced to submicron to nanometer range by using cetyltrimethylammonium bromide (CTAB) and long chain poly(ethylene) glycol (mainly PEG 20,000) as modulators (Liu et al., 2016). However, both the modulators, CTAB and PEG with bulky molecular structure exhibit strong interaction with CD cavity and therefore, their complete removal from the highly cross-channel network is not possible even after extensive washing. It has been reported that β-CD can form inclusion complex with CTAB molecules spontaneously and this can be mainly attributed to the hydrophobic interaction between the inner cavities of β-CD and the alkyl chain of CTAB (Bagheri and Rafati, 2014). Likewise, interaction between β-CD and PEG molecules has been also reported in aqueous solution *via* the formation of strong intermolecular hydrogen bonding (Valero et al., 2003). The presence of these bulky molecular chains could affect their physiochemical properties such as their surface area and pore blockage, ultimately affecting their drug/nanoparticles loading efficacy. Also, CTAB is a highly cytotoxic material with well-known degradation effect on bio membranes. CTAB coated gold nanorods was found to be highly toxic on skin cells due to the residual CTAB molecules (Wang et al., 2008). Also, the cells viability test confirmed the significant cytotoxicity against human colon cancer cells (65-75% loss of viability) when it was exposed to CTAB-capped gold nanorods solution (Alkilany et al., 2009). Overall, use of these toxic and bulky molecular chains hinders

the potential application of CD-MOF in biomedicine, and therefore, a safe alternative is required to utilise their excellent inherent biocompatible structure.

We envisage that the replacement of CTAB and PEG 20,000 with safe and low-molecular-weight modulator could help improving the physicochemical properties of CD-MOF which will ultimately lead to the enhanced antimicrobial efficacy of silver loaded framework. After screening the list of modulators that could fit into our hypothesis, we observed that triethylamine (TEA), is the best alternative (Rodríguez et al., 2020; Usman et al., 2020) as it is a safe molecule which is used in some of the cosmetic products related to skin and hair (Fiume et al., 2013), and can be easily removed from the CD-MOF nanocavities due to its volatile nature and small molecular size (molecular weight, 101.19 g/mol). TEA has been used as a capping agent to stabilize the nanoparticles and its role to promote nucleation is well established in MOF (Li et al., 1999; Wang et al., 2018). The effect of TEA on the size reduction of AgNPs was also reported (Wu and Hsu, 2011). Herein, we report the sustainable synthesis and size modulation of CD-MOF by using TEA as a modulator for the first time. Furthermore, AgNPs were synthesised inside the nanocavities of newly synthesised CD-MOF and compared to those obtained using CTAB and PEG as modulators for its antimicrobial efficacy (tested against *Staphylococcus aureus* and *Escherichia coli* bacteria and *Candida albicans* fungus) and other important characteristics such as surface area and nanoparticles loading efficiency. Their antimicrobial efficacy was assisted by the agar cut well method and minimal inhibitory concentration (MIC) herein.

2. EXPERIMENTAL

2.1. Materials & Regents

The γ-cyclodextrin (γ-CD, 98%) was purchased from Apollo Scientific (UK). Regent grade, 90% potassium hydroxide (KOH), molecular biology grade, ≥99% cetyltrimethylammonium bromide (CTAB), poly(ethylene) glycol 20000 (PEG), HPLC grade absolute ethanol (EtOH), acetonitrile (anhydrous, ≥98%), and HPLC grade, ≥99% methanol (MeOH), ≥99.5% triethyl-amine (TEA) and silver nitrate ($AgNO_3$) ACS reagent (≥99%) were purchased from Sigma-Aldrich (UK). For the antimicrobial tests, laboratory strain bacteria, *S. aureus* and *E. coli*, and fungi *C. albicans* (ATCC 2091) were kindly provided by The University of Hertfordshire microorganism collection. Also, 25% glutaraldehyde in H_2O, 4% osmium tetroxide in H_2O, nutrient agar, yeast peptone dextrose agar, nutrient broth, yeast peptone dextrose broth, Mueller Hinton broth and resazurin dye (Bioreagent grade) were purchased from Sigma-Aldrich (UK). (x10) phosphate buffered saline (Invitrogen (TM)) was obtained from Thermo Fisher Scientific (UK).

2.2. Synthesis of CD-MOF-TEA

CD-MOF nanoparticles were synthesised according to the previously reported methods (Liu et al., 2016; Singh et al., 2017b) with some modifications to make it

more biofriendly. An aqueous solution (10 mL) of γ-CD (324 mg, 25 mM) and KOH (112 mg, 200mM) was prepared. Then, 1 mL of MeOH was directly added to the glass vial and heated for 30 minutes at 70 °C and then different amounts of TEA (1 mL – 3.0 mL) was added followed by the addition of equal amount of MeOH as parent solution. The suspension was incubated at room temperature for 2 hr. Finally, the precipitates were harvested using a centrifuge (5000 RPM) and repeatedly washed three times with EtOH and dried at 50°C overnight under vacuum.
Control CD-MOF samples with CTAB and PEG and CD-MOF particles (without any modulator) were synthesised by replicating methods reported previously (Liu et al., 2017) and the detailed synthesis procedure is presented in the supporting information. For clarity, CD-MOF synthesised using TEA, CTAB, or PEG is termed as CD-MOF-TEA, CD-MOF-CTAB and CD-MOF-PEG, respectively. Large millimtere sized CD-MOF particles have been obtained by slow introduction of MeOH vapours into aqueous solution of γ-CD and KOH at 50 °C for 3-4 days (Smaldone et al., 2010).

2.3. *In situ* synthesis of AgNPs inside CD-MOF

For *in-situ* synthesis of AgNPs, CD-MOF crystals were first immersed in acetonitrile for 72 hr (for solvent exchange) followed by replacement with 10 mM solution of $AgNO_3$ in acetonitrile. Typically, 200 mg of CD-MOF particles were immersed in 10 mL acetonitrile solution of 10 mM $AgNO_3$ for 72 hours. The as-prepared Ag-CD-MOF particles were collected from the reaction solution using a centrifuge (5000 RPM), washed with acetonitrile several times and then left overnight for vacuum dry at 40 °C.

2.4. Characterizations

The samples were scanned for their morphologies using scanning electron microscope (SEM) on Zeiss XB1540 Crossbeam system. The sample powders were fixed on a metal stub using an adhesive carbon tape and then coated with a thin gold film before SEM examination at 5 kV voltage and 10 mA current. The size of the nanoparticles was analysed using commercial ImageJ software. Fourier-transform infrared spectroscopy (FTIR) spectra were recorded with a spectrophotometer (Spectrum Two^{TM}, Perkin Elmer) in the region of 600 to 4000 cm^{-1} in the absorption mode.

Nitrogen adsorption-desorption isotherm for CD-MOF samples were measured using a porosimeter (TriStar 3000 V6.05 A, USA). CD-MOF-TEA, CD-MOF-CTAB, and CD-MOF-PEG were firstly activated by immersing in chloroform for three days and dried under vacuum at 50 °C for 12 hr to remove the entrapped solvents. Specific amounts of samples (e.g. 150-200 mg) were loaded into the sample tubes and degassed under vacuum (10-5 Torr) at 100 °C for 5 hr to remove any gas or solvent traces from the MOF cavities. Based on the gas adsorption efficiency (N_2 in this

case), specific surface area of the samples was calculated in area units per mass of sample (m^2/g) using Brunauer, Emmett and Teller (BET) model. The thermal properties of the samples based on weight change in relation to heating at constant temperature were characterised using Discovery TGA (TA Instruments, USA). For TGA, samples (~5-10 mg) were placed in open aluminium pans and were heated from 40 °C - 500 °C with a ramp of 10 °C/min. They were subsequently purged under a flux of nitrogen gas. The percentage of weight losses and onset thermal degradation temperatures were recorded from the TGA traces obtained.

The AgNPs embedded in CD-MOF samples were characterised using transmission electron microscopy (TEM) on JEOL 2100 200 KV system fitted with a LaB6 filament giving a point resolution of 0.13 nm operated on bright-field mode. The samples were dispersed in water to release the AgNPs and deposited into holey TEM copper grids. The morphology and size of the AgNPs were estimated using ImageJ software. To study the effect of modulators on the stability of AgNPs, samples in the form of suspension were stored at different temperatures, 4 °C, 25 °C, and 37 °C for at least 1 month. The suspension was prepared by dissolving Ag-CD-MOF in water at concentration of 1000 µg/mL. The stability was assisted by UV-Vis spectrometry (UV-Vis 3800). The UV–Vis spectrum were acquired in the 300–800 nm range and the distinct wavelength of UV or visible light absorbed by AgNPs in comparison to control was used to calculate the concentration of nanoparticles. A water sample without any Ag-CD-MOF was used as a control during the measurement. The UV spectra graphs were obtained using Origin Pro 2021 and the position of surface plasmon resonance (SPR) peaks were monitored. Zeta potential and size of the CD-MOF particles were measured using Malvern Panalytical ZetaSizer (model Zen3600) using dynamic light scattering technique which operates on photon auto-correlation function. For zeta potential, powder samples were dispersed at concentrations of 0.1, 0.01 and 0.001 wt/v% in water and measured 3 times with 100 measurements per time. For particle size, CD-MOF were dispersed in absolute ethanol at concentration of 1000 µg/mL and measured 3 times with 15 measurements per time. Water without samples was used as a control.

2.5. Antimicrobial tests

To assess the antimicrobial activity of the CD-MOF crystals containing silver nanoparticles, agar cut well method and MIC tests were performed. Laboratory strain bacteria, *S. aureus* and *E. coli*, and fungi *C. albicans* (ATCC 2091) were grown in nutrient and yeast peptone dextrose broth, respectively.

Agar cut well method: Microbes were diluted to ~1-3 x 10^7 colony forming units (CFU/mL) and inoculated onto Mueller Hinton agar plates. Wells (4 mm in diameter) were cut and sample suspensions at the concentration of 1000 µg/mL were added. Plates were incubated and the diameter of the zone of inhibition was measured (in cm).

Minimal inhibitory concentration (MIC) tests: To investigate the MIC, sample suspensions were diluted to form a final concentration gradient from 500 µg/mL to

7.8 µg/mL. An antibiotic control was included to assess the antibiotic resistance of microbial strains. Then the plate was incubated with ~1-3 x 10^4 CFU/mL of microbes. Resazurin indicator dye was added and further incubated before assessing the colour change; the lowest concentration that did not change in colour was regarded as the MIC. An example of the plate template and resazurin colour change after 24 hours is displayed in supplementary Fig. S1. All incubation was done at 37 ^oC for 24 hours.

In addition, growth inhibition of the microbes with Ag-CD-MOF-TEA treatment was also investigated for 24 hours. An initial 1000 µg/mL concentration was added to the well plate diluted to a final concentration of 250 µg/mL - 1.95 µg/mL (supplementary Fig. S1). Microbes were diluted to ~1-3 x 10^4 CFU/mL and incubated at 37 ^oC with the different concentrations of dispersed sample suspension in quadruplets. Absorbance of the samples was measured every hour using ClarioStar spectrometer at 600 nm with orbital shaking of sample plate for 5 seconds at 100 rpm prior to each measurement. Initial absorbance was used a blank taken away from the corresponding data and the mean of replicates was calculated and plotted as a growth kinetic graph, with error bars denoted as standard deviation.

3. RESULTS & DISCUSSION

3.1. Size modulation of CD-MOF using TEA

TEA is used for the first time to replace the bulky and toxic modulators, CTAB and PEG 20,000 from synthesis of nanosized CD-MOF (Fig. 1). When observed under microscope, cracks were observed on the surface of large CD-MOF crystals synthesised (Fig. 2A). Since the introduction by Liu et al., in 2016, CTAB and PEG 20,000 have been used quite a lot to obtain nanosized particles of CD-MOF (He et al., 2021; Liu et al., 2016). In this study, we introduce safer modulator, TEA and the morphology of CD-MOF-TEA in comparison with CD-MOF-CTAB and CD-MOF-PEG samples is presented in Fig. 2B, 2C and 2D, respectively. A typical cubic shape could be observed in all samples with no significant difference between all the three modulators. However, it is important to note that the use of TEA has resulted in a faster solvothermal synthesis where crystallisation is completed in 1-2 hours compared to 6-12 hr long process with other modulators and the synthesis time is in days when no modulator was used (Liu et al., 2016; Singh et al., 2017b; Smaldone et al., 2010). This could be attributed to the well-understood role of TEA to facilitate the crystallisation by enhancing deprotonation of organic ligands, cyclodextrin in this case. The deprotonation of hydroxyl functional groups of cyclodextrin using base has been confirmed previously and which might be the reason for faster synthesis of CD-MOF using TEA (Gaidamauskas et al., 2009).

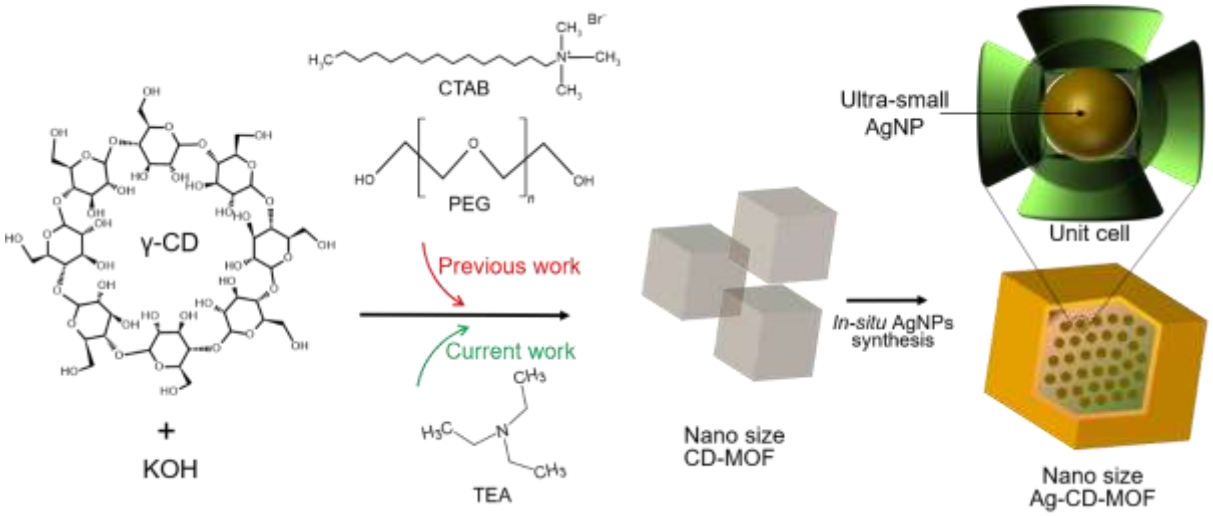

Figure 1 Schematic showing the new synthesis of CD-MOF with TEA as modulator followed by in-situ synthesis of silver nanoparticles inside formwork using MOF cavities as nanoreactors for the silver salt reduction.

To understand the effect, the concentration of TEA was varied from 0 to 3 mL. A significant effect of TEA concentration on the size and crystal uniformity was observed where the size of the CD-MOF particles reduced from ~2 µm to ~254 nm when the concentration was increased from 1 to 3 mL, respectively (supplementary Fig. S2). When compared to original millimetre sized crystals, relatively smaller particles with an average size of ~3 µm was obtained in the sample where the concentration of TEA was 0 mL which could be due to the excess of MeOH (10 mL). However, the crystals were non-uniform with size ranging from ~200 nm to as big as ~13 µm. At 3 mL concentration of TEA, the average size of the CD-MOF nanoparticles was measured ~254 nm while the average size of the nanoparticles from PEG 20,000 and CTAB modulators was measured ~282 and ~278 nm, respectively. According to the data obtained from varying TEA amount (supplementary Fig. S2) 3 mL is used as the final optimised concentration for further study. Hydrodynamic diameters of the CD-MOF crystal measured using DLS was recorded in higher range (>1 µm), might be due to the particle aggregation when suspended in EtOH (supplementary Fig. S3). The chemical structure of the CD-MOF crystals was confirmed using FTIR (supplementary Fig. S4, and Fig. 2E). Typical CD-MOF characteristic FTIR peaks at 3000-3500 cm^{-1} and 800-1000 cm^{-1} corresponding to -OH group's stretching vibration in the glucose ring and C-H bending vibration were recorded in all samples (Fig. 2E). However, when observed carefully, a sharp low intensity additional peak at 2970 cm^{-1} was observed in CD-MOF-CTAB samples which correspond to methyl group ($-CH_3$) of CTAB, further supporting our claim of forming inclusion complex between CTAB and γ-CD (supplementary Fig. S5) (Su et al., 2015). Due to chemical structure similarity between PEG and CDs, no additional peak was observed in FTIR spectra of PEG modulated samples. The absence of C-N stretching vibration peak confirmed the complete removal of TEA from CD-MOF frameworks. The MOF crystals from

different modulators were further compared for their surface area and the obtained N_2 isotherm curves for CD-MOF-CTAB, CD-MOF-PEG, and CD-MOF-TEA are presented in Fig. 2F. The shape of the three isotherm curves is similar to the BET isotherm type 1, which refers to the microporous solid (pores with <2 nm). CD-MOF-TEA exhibited the highest BET surface area of 1075.5 m^2/g when compared to those obtained from CTAB (455.12 m^2/g) and PEG (493.6 m^2/g). These results again suggested that the remained polymer chains adversely affected the physicochemical properties of CD-MOF. When compared with the literature, it shows that TEA has not affected the surface area which is comparable to CD-MOF synthesized without any modulator (Smaldone et al., 2010). The reason for higher surface area in TEA modulated samples could be explained by the physicochemical characteristics of base. TEA is volatile organic compound (VOC) which could be easily evaporated and/or washed out with solvents due to its high vapor pressure and polarity and low molecular weight (Zhang et al., 2021).

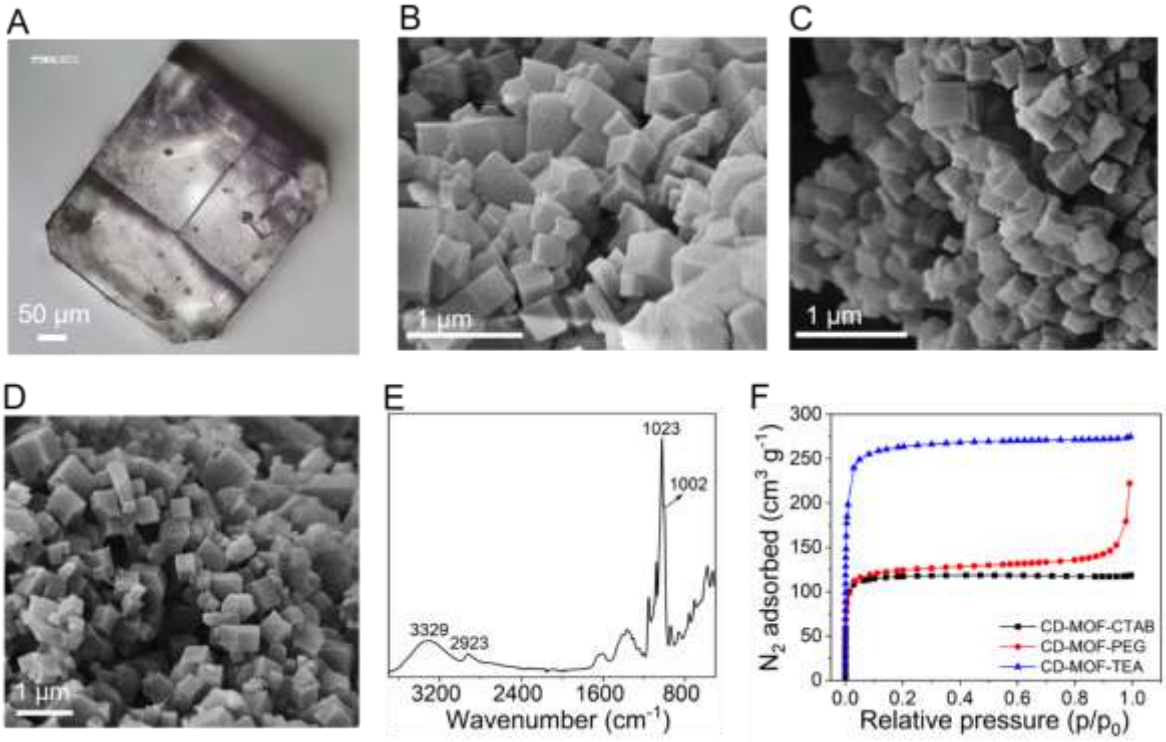

Figure 2 CD-MOF characterisation. (A) Optical microscopy image of a large CD-MOF crystal synthesised by state-of-the-art vapor diffusion method. (B) SEM images of the cubic nanoparticles of CD-MOF-CTAB, (C) CD-MOF-PEG and (D) CD-MOF-TEA. (E) FTIR spectra of CD-MOF-TEA with the indicated characteristic peaks for -OH group's stretching vibration (3000 – 3500 cm^{-1}) and C-H bending vibration (800 – 1000 cm^{-1}). (F) N_2 adsorption isotherms for CD-MOF-CTAB, CD-MOF-PEG and CD-MOF-TEA.

3.2. *In-situ* synthesis of AgNPs inside CD-MOF

Benefitting from sustainable synthesis and high surface area, the cavities of CD-MOF-TEA crystals were used as nanoreactors for the synthesis of ultra-small AgNPs. The synthesis procedure is adopted from previously published reports (Shakya et al., 2019; Wei et al., 2012). The colour of the CD-MOF crystals turned brown-black after silver synthesis (supplementary Fig. S6) and the morphology and crystallinity were recorded using SEM and PXRD, respectively. In-situ growth of the AgNPs did not affect the shape and size of the CD-MOF-TEA crystals (Fig. 3A). The powder was further scanned for the elemental distribution using SEM-EDS (Fig. 3B, 3C and supplementary S7). The sample displays a homogenous distribution of silver which indicated a uniform synthesis of AgNPs within the CD-MOF-TEA framework structure. CD-MOF-CTAB and CD-MOF-PEG samples were also used for AgNPs synthesis for the comparative purpose, which are termed as Ag-CD-MOF-CTAB and Ag-CD-MOF-PEG, respectively. The percentage of each element that was acquired using EDS is presented in (supplementary Table S1). The total percentage of silver was recorded slightly higher in CD-MOF-TEA in comparison to Ag-CD-MOF-CTAB and Ag-CD-MOF-PEG. Spherical shape with 2-5 nm size (average size calculated by ImageJ) was observed under TEM for AgNPs synthesised inside CD-MOF-TEA cavities (Fig. 3D). No significant difference was recorded in the size of AgNPs synthesised inside CD-MOF samples modulated with TEA, CTAB and PEG (supplementary Figure S8). The crystal structure of the Ag-CD-MOF-TEA remained intact with diffraction peaks recorded at same positions as CD-MOF-TEA samples (Fig. 3E). When characterised using FTIR, the spectrum of both, Ag-CD-MOF-TEA and CD-MOF-TEA were found identical supplementary Figure S9 (21).

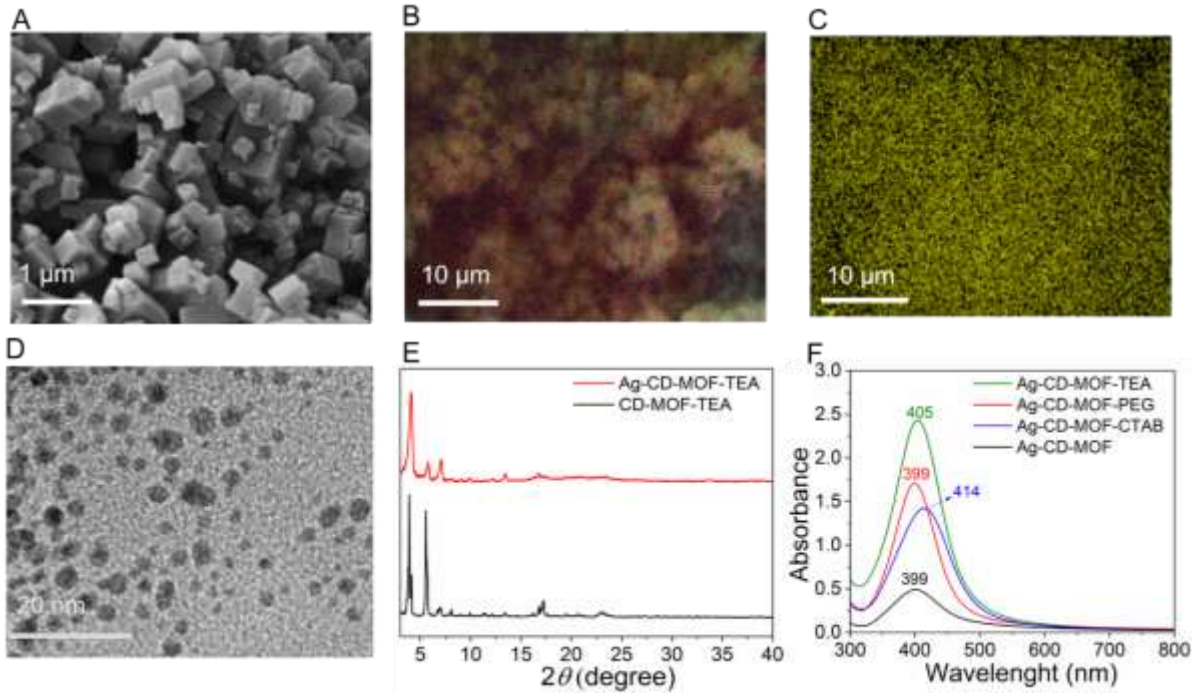

Figure 3: Characterisation of CD-MOF after in-situ silver nanoparticle synthesis. (A) SEM images of the cubic Ag-CD-MOF-TEA. (B) EDS elemental mapping of oxygen (O), potassium (k) and carbon (C). (C) EDS elemental mapping of Ag on the Ag-CD-MOF-TEA nanoparticles. (D) TEM image of AgNPs from CD-MOF-TEA sample. (E)

PXRD characterisation of CD-MOF-TEA and Ag-CD-MOF-TEA. (F) UV-Vis spectra of AgNPs synthesised in CD-MOF-TEA, CD-MOF-PEG, CD-MOF-CTAB and CD-MOF.

AgNPs synthesised in CD-MOF samples were detected under UV-Vis spectroscopy. The UV-Vis spectrum of AgNPs synthesised in CD-MOF-TEA, CD-MOF-CTAB, CD-MOF-PEG and CD-MOF are shown in Fig. 3F. The wavenumber of the SPR peak can provide the information about the size of AgNPs, and the peak would shift towards lower wavenumber with decreasing AgNPs size (Paramelle et al., 2014). The SPR peaks for Ag-CD-MOF and Ag-CD-MOF-PEG were detected at 399 nm while the SPR peak for Ag-CD-MOF-TEA was detected at slightly higher wavenumber of 405 nm. The SPR peak for Ag-CD-MOF-CTAB was detected at much higher wavenumber of 414 nm. The obtained results suggested that the AgNPs released from CTAB modulated samples tend to aggregate, might be due to the formation of inclusion complex between CTAB and the hydrophobic cavities of cyclodextrin units.

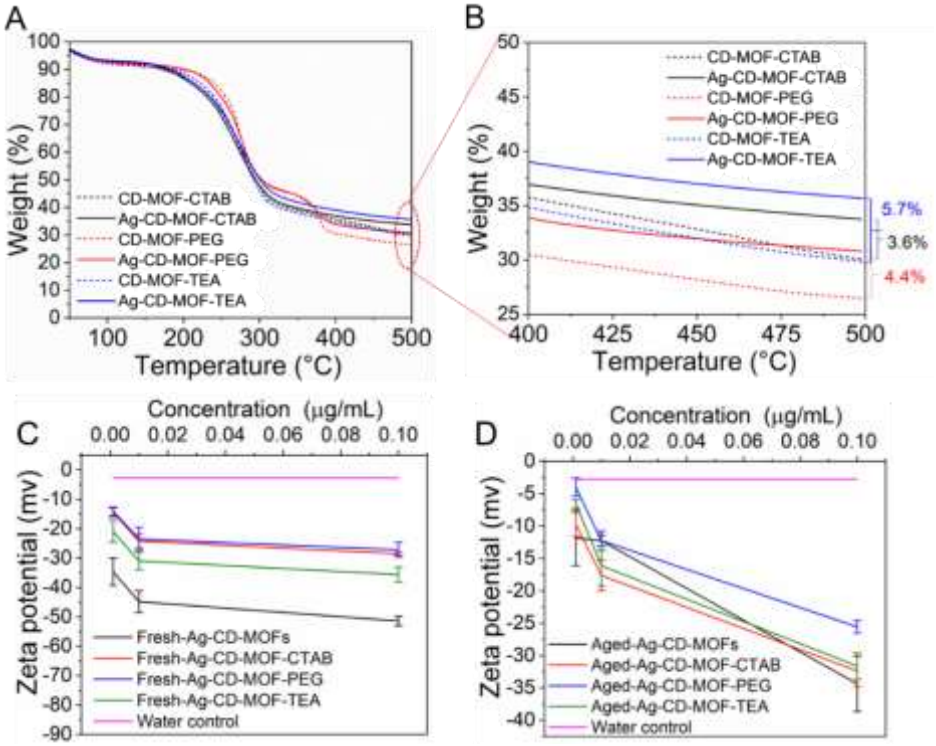

Figure 4 Silver quantification and Zeta potential measurements. (A & B) TGA curves of CD-MOF and (B) AgNPs synthesised within CTAB, PEG & TEA modulated CD-MOF with zoom in version of the same graph to visualise the clear difference in the remaining weight which correspond to the concentration of silver nanoparticles. (C) Zeta potential of fresh samples and (D) aged samples (after 30 days) of Ag loaded CD-MOF synthesised using different modulators.

AgNPs loaded samples were subjected to thermal gravimetric analysis (TGA) to confirm the presence of polymers (surfactants) residue and investigate the amount of

AgNPs inside the framework. TGA curves for CD-MOF-TEA and CD-MOF-CTAB showed identical thermal decomposition behavior (Fig 4A). The first thermal decomposition at 50 °C - 100 °C possibly represents the evaporation of the trapped solvents in the nanocavities of CD-MOF. The second decomposition at around 175 °C, could be mainly because of the degradation of γ-CD units (Smaldone et al., 2010). A similar trend was recorded for CD-MOF-PEG sample except for the decomposition of γ-CD was delayed until around 220 °C. This could be explained by stabilisation affect from polymer chains on the MOF structure (Li et al., 2014) which confirmed the un-complete removal of PEG chains from CD-MOF nanocavities. The TGA curve of CD-MOF-PEG presented another decomposition stage started at around 364 °C which could be attributed to PEG degradation (Irfan Khan et al., 2015). Fig. 4A shows the TGA curves of silver loaded CD-MOF samples, Ag-CD-MOF, Ag-CD-MOF-TEA, Ag-CD-MOF-CTAB and Ag-CD-MOF-PEG. The overall thermal stability of all the four samples remained unaffected after the synthesis of AgNPs. The difference between the remaining weight of CD-MOF-TEA and Ag-CD-MOF-TEA recorded around 5% which could be accounted for AgNPs. The weight % of AgNPs in Ag-CD-MOF-TEA recorded highest (5.7%) when compared with the 4.4%, 3.6% and 1% in Ag-CD-MOF-PEG, Ag-CD-MOF-CTAB and Ag-CD-MOF, respectively (Fig. 4B). Additionally, the UV-Vis absorbance of AgNPs was compared from all three samples and as expected, highest absorbance intensity was recorded from Ag-CD-MOF-TEA sample which again supported the claim that high surface area enhanced the AgNPs loading (Fig. 3F).

3.3. Stability of AgNPs synthesised inside CD-MOF particles

After successful synthesis of ultra-small AgNPs inside CD-MOF-TEA, the stability of the nanoparticles was assessed using Zeta potential and UV-Vis spectroscopy for 30 days of storage at 4 °C, 25 °C and 37 °C. As shown in Fig. 4C, an increase in the concentration of silver loaded crystals increased the zeta potential values, with -51.37±1.64 mV, -35.6±2.5 mV, -28.5±0.5 mV and -27.13±2.45 mV was recorded for Ag-CD-MOF, Ag-CD-MOF-TEA, Ag-CD-MOF-CTAB and Ag-CD-MOF-PEG, respectively. Zeta potential of -2.7 mV was measured for the deionized water (control). Zeta potential is the measurement of the electrostatic charge on the surface of particles; values outside the ±20-30 mV range is regarded as stable due to the charged particles' ability to repel, thus unlikely to form agglomerates (Mourdikoudis et al., 2018). After dissolving MOF crystals in water, AgNPs released from CD-MOF cavities would be stabilized by CD-units (Wei et al., 2012). The hydrophobic cavities of CD, which is well-known for its inclusion forming capabilities, forms host–guest interaction with nanoparticles and help them stabilise in the suspension (Huang et al., 2009). According to the obtained zeta potential values of -35.6 mV, Ag-CD-MOF-TEA can form the most stable suspension and AgNPs are unlikely to form agglomerates. The zeta potential of Ag-CD-MOF-PEG and Ag-CD-MOF-CTAB is slightly closer to the instability range - might be due the competition between residual polymer chains and AgNPs to form inclusion complex with CD

units. Nevertheless, the obtained data suggested that all samples can form stable suspension in water. The zeta potential of Ag-CD-MOF-TEA suspension decreased slightly to -31.6 ± 2.05 mV after storing it for 30 days at 25 °C (Fig. 4D). Similar trend was observed in Ag-CD-MOF and Ag-CD-MOF-PEG suspensions. Interestingly, the zeta potential was increased from -28.5 ± 0.5 to -32.2 ± 2 for stored Ag-CD-MOF-CTAB suspension. This could be attributed to nanoparticle agglomeration. It was observed that the colour of Ag-CD-MOF suspension turned darker (supplementary Fig. S10) due to the agglomerates formation which did not contributed towards the zeta potential measured.

Furthermore, the stability of the fresh and stored suspensions (30 days) was also assessed using UV-Vis spectroscopy. The obtained data is presented as supplementary Fig. S11. Ag-CD-MOF-TEA samples demonstrated excellent stability at 4 °C, 25 °C and 37 °C tested for 30 days. The SPR peak of the samples stored at 25 °C and 37 °C showed a slight shift to the higher wavenumber after one week of storage, and no change was observed in the sample stored at 4 °C. The shift became larger for all the three samples which indicate that the size of AgNPs increased slightly due to agglomeration. Both Ag-CD-MOF and Ag-CD-MOF-PEG showed good stability as the SPR peak shifted slightly to higher wavenumbers after one week. However, the samples stored at 37 °C shows a greater shift after 30 days compared to the other samples. AgNPs synthesised in CD-MOF-CTAB were found to be less stable than those synthesised from other modulators with quick aggregation was observed (supplementary Fig. S9), this might be due to the highly stable inclusion complex formation between CD units and CTAB which affected the stabilisation capabilities of CD (Bagheri and Rafati, 2014).

3.4. Antimicrobial test results

The antimicrobial efficacy of Ag-CD-MOF-TEA was tested against bacteria, *S. aureus* and *E. coli*, and fungi *C. albicans* and compared with Ag-CD-MOF-PEG and Ag-CD-MOF-CTAB. Zone of inhibition diameters (ZOI) and overall MIC was used as the measurement standards. MIC and ZOI measured for different samples are presented as Fig. 5A and Table 1 respectively. Ag-CD-MOF-TEA has the highest antimicrobial efficacy in ZOI and showed excellent antifungal activity based on the obtained MIC results (31-15 µg/mL) when compared to the other samples. The enhanced antimicrobial ability of the newly synthesised Ag-CD-MOF-TEA could be attributed to the improved physiochemical properties of CD-MOF, especially, the surface area which led to high AgNPs yield confirmed in above sections. However, the mechanism of action for Ag is not completely understood yet, but it is elucidated that Ag^+ ions can i) puncture the cell wall by reacting with the peptidoglycan component, ii) inhibit the cellular respiration and disrupt the metabolic pathways through generation of reactive oxygen species and iii) also disrupt the DNA and its replication cycle Ag^+ and their subsequent interaction and damage (Le Ouay and Stellacci, 2015).

Table 1: The MIC of Ag-CD-MOF synthesised with TEA, CTAB, PEG, and without a modulator against *E. coli, S. aureus* and *C. albicans*.

Sample	***E. coli* (µg/mL)**	***S. aureus* (µg/mL)**	***C. albicans* (µg/mL)**
CD-MOF	500-250	>500	500
Ag-CD-MOF	125	125	500
Ag-CD-MOF-CTAB	62-31	250-125	62-31
Ag-CD-MOF-PEG	62-31	250-125	62-31
Ag-CD-MOF-TEA	62-31	250-125	31-15

The comparatively low antimicrobial efficacy of Ag-CD-MOF-CTAB samples could be due to the larger size of AgNPs as confirmed earlier. The large particles of Ag-CD-MOF showed no antimicrobial activity when tested using the cut well method, and required higher concentrations to have an effect, if any, when tested for their MIC. This could be due to two reasons, the inability of larger MOF particle size (> 100 µm) to penetrate and slow frameworks degradation which might have affected the release of Ag^+ ions. The second reason could be the less silver concentration inside CD-MOF, again due to slow diffusion of the solvent (containing silver precursor) inside crystals during *in situ* synthesis.

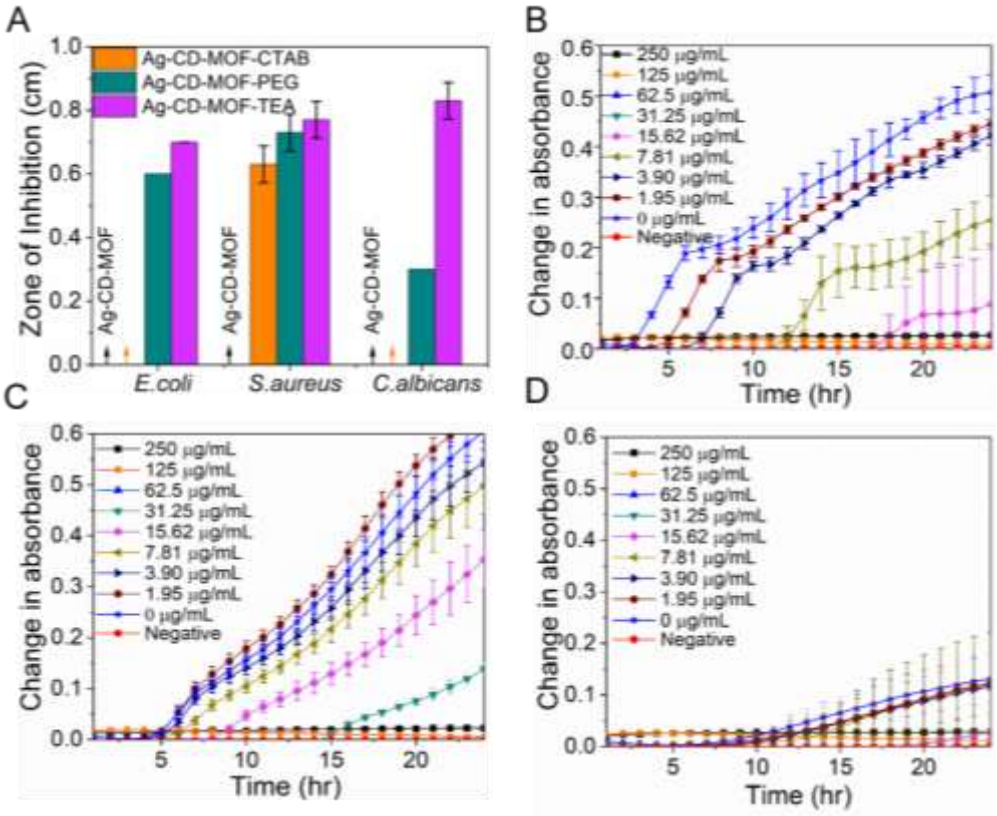

Figure 5 Antimicrobial testing (A) Zone of inhibition diameter (in cm) of Ag-CD-MOF synthesised with different modulators against bacteria and fungi, (B) the growth kinetic of *E. Coli* (C), *S. aureus*, (D) and, fungi *C. albicans* treated with various concentrations of Ag-CD-MOF-TEA was monitored over 24 hours.

The growth kinetics of microbes treated with various concentrations of Ag-CD-MOF-TEA was monitored over a 24 hr period with an optical density reading taken every hour. As shown in Fig. 5 (B, C & D), the growth kinetics of the microbes*, E. Coli S. aureus, and, fungi C. albicans* was found concentration-dependent. Even at lower concentrations, Ag-CD-MOF-TEA was able to slightly reduce and delay the growth, whilst higher concentrations were able to completely inhibit the microbial growth. The results showed that 62 µg/mL and higher concentration were able to inhibit 100% growth of all three microbial when treated with Ag-CD-MOF-TEA. However, resazurin assay indicated that the MIC was higher against some of the microbes. A reason for the slight difference in results could be that the growth of microbes was inhibited by the Ag-CD-MOF-TEA, however the cells were still metabolically active, thus were able to reduce resazurin leading to a colour change. *S. aureus* is associated with two-thirds of the orthopaedic implant infections and these infections are difficult to treat as the bacteria always tend to form biofilm (Ribeiro et al., 2012). Prashik et al., reported the MIC values of AgNPs - with an average size of 5 nm produced from nanoComposix company against *S. aureus* as 0.625 mg/mL which is very high compared to Ag-CD-MOF (Parvekar et al., 2020). Therefore, the AgNPs synthesised within CD-MOF matrix especially CD-MOF-TEA can provide a potent

antimicrobial effect with very low concentration of AgNP as indicated by the MIC values.

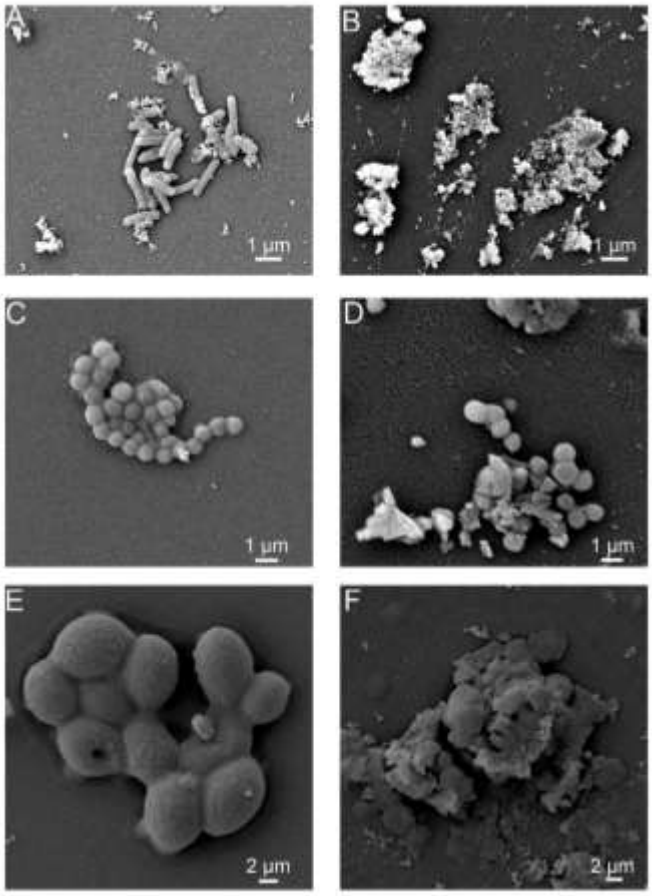

Figure 6 SEM images of control and treated samples (A) *E. Coli* control, (B) *E. Coli* treated with Ag-CD-MOF-TEA. (C) *S. aureus* control and (D) *S. aureus* treated with Ag-CD-MOF-TEA. (E) *C. albicans* control and *C. albicans* treated with Ag-CD-MOF-TEA.

The SEM images of the healthy microbes (*E. coli, S. aureus* and *C. albicans*) and treated with Ag-CD-MOF-TEA are presented in Fig. 6. The disruption of cell wall with extensive cellular debris could be observed in all three cases, where the effect on *E. coli* was the highest. Furthermore, the effect of the silver loaded CD-MOF on the size of microbes (those managed to survive) was also tested. The size of at least 20 healthy cells was measured in each case using ImageJ (supplementary Fig. S12). The average size of the untreated *E. coli* was recorded 2.3±0.7 µm which was reduced to 1.6±0.4 µm after the treatment. Similar effect was also recorded where the size of *S. aureus* and *C. albicans* were reduced from 0.8±0.1 µm and 4.7±0.7 µm to 0.69±0.1 µm and 2.2±1.5 µm, respectively. The obtained results suggested the excellent antimicrobial activity of the silver nanoparticles released from highly aligned frameworks of CD-MOF which successfully prevented the aggregation of the nanoparticles in solution (treated medium).

4. Conclusion

In this research, we proposed TEA as a modulator to improve the physicochemical characteristics and hence, the antimicrobial efficiency of silver loaded CD-MOF by replacing conventional high-molecular-weight PEG 20,000 and cytotoxic CTAB from the synthesis. The obtained results show that TEA can be used an alternative for the rapid synthesis of uniform nanosized CD-MOF crystals. CD-MOF prepared using TEA as a modulator demonstrated higher specific surface area (1075.5 m^2/g) compared to the samples synthesised with CTAB (455.12 m^2/g) and long chain PEG (493.6 m^2/g). TEA modulated crystals used for synthesising ultra-small AgNPs has resulted in enhanced antimicrobial efficacy tested against both, bacteria and fungus. The improved CD-MOF skeleton led to high silver nanoparticles payload, 58.3%, 29.5% and 470% increase is measured when compared to CD-MOF synthesised without any modulator, with CTAB and PEG, respectively. Increment in ZOI diameters is also observed against all the tested microbes, specifically, the MIC towards fungi *C. albicans* significantly enhanced (31-15 µg/mL) compared to those obtained from CTAB (62-31 µg/mL) and PEG (62-31 µg/mL). Based on the above results, we strongly believe that this study could be very useful in further exploration of these newly synthesised CD-MOF crystals in biomedicine field.

5. Acknowledgment

This study was supported by the outcomes of Engineering and Physical Sciences Research Council funding (EP/N034368/1), and Royal Society (IEC\NSFC\201155). E.C. would like to thank the scholarship from University of Hertfordshire.

6. References

Agnihotri, S., Mukherji, S., and Mukherji, S. (2014). Size-controlled silver nanoparticles synthesized over the range 5–100 nm using the same protocol and their antibacterial efficacy. *RSC Advances 4*, 3974-3983.

Akter, M., Sikder, M.T., Rahman, M.M., Ullah, A.K.M.A., Hossain, K.F.B., Banik, S., Hosokawa, T., Saito, T., and Kurasaki, M. (2018). A systematic review on silver nanoparticles-induced cytotoxicity: Physicochemical properties and perspectives. *Journal of Advanced Research 9*, 1-16.

Alkilany, A.M., Nagaria, P.K., Hexel, C.R., Shaw, T.J., Murphy, C.J., and Wyatt, M.D. (2009). Cellular uptake and cytotoxicity of gold nanorods: molecular origin of cytotoxicity and surface effects. *Small 5*, 701-708.

Andrieux-Ledier, A., Tremblay, B., and Courty, A. (2013). Stability of self-ordered thiol-coated silver nanoparticles: oxidative environment effects. *Langmuir 29*, 13140-13145.

Bagheri, A., and Rafati, A.A. (2014). Thermodynamic investigation of inclusion complex formation between cetyltrimethyl ammonium bromide (CTAB) and β-cyclodextrin at various temperatures. *Journal of Molecular Liquids 195*, 145-149.

595 Cao, J., Yang, Z., Xiong, W., Zhou, Y., Wu, Y., Jia, M., Zhou, C., and Xu, Z. (2021). Ultrafine
596 metal species confined in metal–organic frameworks: fabrication, characterization and
597 photocatalytic applications. *Coordination Chemistry Reviews 439*, 213924.
598
599 Cure, J., Mattson, E., Cocq, K., Assi, H., Jensen, S., Tan, K., Catalano, M., Yuan, S., Wang,
600 H., Feng, L.*, et al.* (2019). High stability of ultra-small and isolated gold nanoparticles in
601 metal–organic framework materials. *Journal of Materials Chemistry A 7*, 17536-17546.
602
603 Dakal, T.C., Kumar, A., Majumdar, R.S., and Yadav, V. (2016). Mechanistic basis of
604 antimicrobial actions of silver nanoparticles. *Frontiers in Microbiology 7*.
605
606 Fernando, I., and Zhou, Y. (2019). Impact of pH on the stability, dissolution and aggregation
607 kinetics of silver nanoparticles. *Chemosphere 216*, 297-305.
608
609 Fiume, M.M., Heldreth, B., Bergfeld, W.F., Belsito, D.V., Hill, R.A., Klaassen, C.D., Liebler,
610 D., Marks, J.G., Shank, R.C., Slaga, T.J.*, et al.* (2013). Safety assessment of
611 triethanolamine and triethanolamine-containing ingredients as used in cosmetics.
612 *International Journal of Toxicology 32*, 59S-83S.
613
614 Fouz, N., Pangesti, K.N.A., Yasir, M., Al-Malki, A.L., Azhar, E.I., Hill-Cawthorne, G.A., and
615 Abd El Ghany, M. (2020). The contribution of wastewater to the transmission of antimicrobial
616 resistance in the environment: implications of mass gathering settings. *Tropical Medicine*
617 *and Infectious Disease 5*, 33.
618
619 Gaidamauskas, E., Norkus, E., Butkus, E., Crans, D.C., and Grincienė, G. (2009).
620 Deprotonation of β-cyclodextrin in alkaline solutions. *Carbohydrate Research 344*, 250-254.
621
622 He, Y., Xiong, T., He, S., Sun, H., Huang, C., Ren, X., Wu, L., Patterson, L.H., and Zhang, J.
623 (2021). Pulmonary targeting crosslinked cyclodextrin metal–organic frameworks for lung
624 cancer Therapy. *Advanced Functional Materials 31*, 2004550.
625
626 He, Y., Zhang, W., Guo, T., Zhang, G., Qin, W., Zhang, L., Wang, C., Zhu, W., Yang, M., Hu,
627 X.*, et al.* (2019). Drug nanoclusters formed in confined nano-cages of CD-MOF: dramatic
628 enhancement of solubility and bioavailability of azilsartan. *Acta Pharmaceutica Sinica B 9*,
629 97-106.
630
631 Hong, X., Wen, J., Xiong, X., and Hu, Y. (2016). Shape effect on the antibacterial activity of
632 silver nanoparticles synthesized via a microwave-assisted method. *Environmental Science*
633 *and Pollution Research 23*, 4489-4497.
634
635 Huang, C., Xu, J., Li, J., He, S., Xu, H., Ren, X., Singh, V., Wu, L., and Zhang, J. (2022).
636 Hydrogen peroxide responsive covalent cyclodextrin framework for targeted therapy of
637 inflammatory bowel disease. *Carbohydrate Polymers 285*, 119252.
638
639 Huang, T., Meng, F., and Qi, L. (2009). Facile synthesis and one-dimensional assembly of
640 cyclodextrin-capped gold nanoparticles and their applications in catalysis and surface-
641 enhanced raman scattering. *The Journal of Physical Chemistry* C *113*, 13636-13642.
642
643 Irfan Khan, M., Azizli, K., Sufian, S., Man, Z., and Khan, A.S. (2015). Simultaneous
644 preparation of nano silica and iron oxide from palm oil fuel ash and thermokinetics of
645 template removal. *RSC Advances 5*, 20788-20799.
646 Larson, E. (2007). Community factors in the development of antibiotic resistance. *Annual*
647 *Review of Public Health 28*, 435-447.
648

Larsson, D.G.J., and Flach, C.-F. (2022). Antibiotic resistance in the environment. *Nature Reviews Microbiology 20*, 257-269.

Lawson, H.D., Walton, S.P., and Chan, C. (2021). Metal–organic frameworks for drug delivery: a design perspective. *ACS Applied Materials & Interfaces 13*, 7004-7020.

Le Ouay, B., and Stellacci, F. (2015). Antibacterial activity of silver nanoparticles: A surface science insight. *Nano Today 10*, 339-354.

Li, C., Li, W., Holler, T.P., Gu, Z., and Li, Z. (2014). Polyethylene glycols enhance the thermostability of β-cyclodextrin glycosyltransferase from Bacillus circulans. *Food Chemistry 164*, 17-22.

Li, H., Eddaoudi, M., O'Keeffe, M., and Yaghi, O.M. (1999). Design and synthesis of an exceptionally stable and highly porous metal-organic framework. *Nature 402*, 276-279.

Li, H., Hill, M.R., Huang, R., Doblin, C., Lim, S., Hill, A.J., Babarao, R., and Falcaro, P. (2016). Facile stabilization of cyclodextrin metal–organic frameworks under aqueous conditions via the incorporation of C60 in their matrices. *Chemical Communications 52*, 5973-5976.

Li, X., Zhao, X., Chu, D., Zhu, X., Xue, B., Chen, H., Zhou, Z., and Li, J. (2022). Silver nanoparticle-decorated 2D Co-TCPP MOF nanosheets for synergistic photodynamic and silver ion antibacterial. *Surfaces and Interfaces 33*, 102247.

Liu, B., He, Y., Han, L., Singh, V., Xu, X., Guo, T., Meng, F., Xu, X., York, P., Liu, Z.*, et al.* (2017). Microwave-assisted rapid synthesis of γ-cyclodextrin metal–organic frameworks for size control and efficient drug loading. *Crystal Growth & Design 17*, 1654-1660.

Liu, B., Li, H., Xu, X., Li, X., Lv, N., Singh, V., Stoddart, J.F., York, P., Xu, X., Gref, R.*, et al.* (2016). Optimized synthesis and crystalline stability of γ-cyclodextrin metal-organic frameworks for drug adsorption. *International Journal of Pharmaceutics 514*, 212-219.

Luzuriaga, M.A., Welch, R.P., Dharmarwardana, M., Benjamin, C.E., Li, S., Shahrivarkevishahi, A., Popal, S., Tuong, L.H., Creswell, C.T., and Gassensmith, J.J. (2019). Enhanced stability and controlled delivery of MOF-encapsulated vaccines and their immunogenic response in vivo. *ACS Applied Materials & Interfaces 11*, 9740-9746.

Mourdikoudis, S., Pallares, R.M., and Thanh, N.T.K. (2018). Characterization techniques for nanoparticles: comparison and complementarity upon studying nanoparticle properties. *Nanoscale 10*, 12871-12934.

Paramelle, D., Sadovoy, A., Gorelik, S., Free, P., Hobley, J., and Fernig, D.G. (2014). A rapid method to estimate the concentration of citrate capped silver nanoparticles from UV-visible light spectra. *Analyst 139*, 4855-4861.

Parvekar, P., Palaskar, J., Metgud, S., Maria, R., and Dutta, S. (2020). The minimum inhibitory concentration (MIC) and minimum bactericidal concentration (MBC) of silver nanoparticles against Staphylococcus aureus. *Biomaterial Investigations in Dentistry 7*, 105-109.

Ribeiro, M., Monteiro, F.J., and Ferraz, M.P. (2012). Infection of orthopedic implants with emphasis on bacterial adhesion process and techniques used in studying bacterial-material interactions. *Biomatter 2*, 176-194.

Rifai, S., Breen, C.A., Solis, D.J., and Swager, T.M. (2006). Facile in situ silver nanoparticle formation in insulating porous polymer matrices. *Chemistry of Materials 18*, 21-25.

Rodríguez, N.A., Parra, R., and Grela, M.A. (2020). Triethylamine as a tuning agent of the MIL-125 particle morphology and its effect on the photocatalytic activity. *SN Applied Sciences 2*, 1881.

Shakya, S., He, Y., Ren, X., Guo, T., Maharjan, A., Luo, T., Wang, T., Dhakhwa, R., Regmi, B., Li, H.*, et al.* (2019). Ultrafine silver nanoparticles embedded in cyclodextrin metal-organic frameworks with GRGDS functionalization to promote antibacterial and wound healing application. *Small 15*, 1901065.

Singh, V., Guo, T., Wu, L., Xu, J., Liu, B., Gref, R., and Zhang, J. (2017a). Template-directed synthesis of a cubic cyclodextrin polymer with aligned channels and enhanced drug payload. *RSC Advances 7*, 20789-20794.

Singh, V., Guo, T., Xu, H., Wu, L., Gu, J., Wu, C., Gref, R., and Zhang, J. (2017b). Moisture resistant and biofriendly CD-MOF nanoparticles obtained via cholesterol shielding. *Chemical Communications 53*, 9246-9249.

Skandalis, N., Dimopoulou, A., Georgopoulou, A., Gallios, N., Papadopoulos, D., Tsipas, D., Theologidis, I., Michailidis, N., and Chatzinikolaidou, M. (2017). The effect of silver nanoparticles size, produced using plant extract from arbutus unedo, on their antibacterial efficacy. *Nanomaterials 7*, 178.

Smaldone, R.A., Forgan, R.S., Furukawa, H., Gassensmith, J.J., Slawin, A.M.Z., Yaghi, O.M., and Stoddart, J.F. (2010). Metal–organic frameworks from edible natural products. *Angewandte Chemie International Edition 49*, 8630-8634.

Staroń, A., and Długosz, O. (2021). Antimicrobial properties of nanoparticles in the context of advantages and potential risks of their use. *Journal of Environmental Science and Health*, Part A *56*, 680-693.

Su, G., Yang, C., and Zhu, J.-J. (2015). Fabrication of gold Nanorods with tunable longitudinal surface plasmon resonance peaks by reductive dopamine. *Langmuir 31*, 817-823.

Torres-Flores, E.I., Flores-López, N.S., Martínez-Núñez, C.E., Tánori-Córdova, J.C., Flores-Acosta, M., and Cortez-Valadez, M. (2021). Silver nanoparticles in natural zeolites incorporated into commercial coating: antibacterial study. *Applied Physics A 127*, 71.

Usman, K.A.S., Maina, J.W., Seyedin, S., Conato, M.T., Payawan, L.M., Dumée, L.F., and Razal, J.M. (2020). Downsizing metal–organic frameworks by bottom-up and top-down methods. *NPG Asia Materials 12*, 58.

Valero, M., Carrillo, C., Rodrı, x, and guez, L.J. (2003). Ternary naproxen:β-cyclodextrin:polyethylene glycol complex formation. *International Journal of Pharmaceutics 265*, 141-149.

Wang, J., Imaz, I., and Maspoch, D. (2022). Metal−organic frameworks: why make them small? *Small Structures 3*, 2100126.

Wang, S., Lu, W., Tovmachenko, O., Rai, U.S., Yu, H., and Ray, P.C. (2008). Challenge in understanding size and shape dependent toxicity of gold nanomaterials in human skin keratinocytes. *Chemical Physics Letters 463*, 145-149.

Wang, S., Lv, Y., Yao, Y., Yu, H., and Lu, G. (2018). Modulated synthesis of monodisperse MOF-5 crystals with tunable sizes and shapes. *Inorganic Chemistry Communications 93*, 56-60.

Wei, Y., Han, S., Walker, D.A., Fuller, P.E., and Grzybowski, B.A. (2012). Nanoparticle core/shell architectures within MOF crystals synthesized by reaction diffusion. *Angewandte Chemie International Edition 51*, 7435-7439.

Wenzel, M. (2020). Do we really understand how antibiotics work? *Future Microbiology 15*, 1307-1311.

Wu, J.-T., and Hsu, S.L.-C. (2011). Preparation of triethylamine stabilized silver nanoparticles for low-temperature sintering. *Journal of Nanoparticle Research 13*, 3877-3883.

Zahn, G., Zerner, P., Lippke, J., Kempf, F.L., Lilienthal, S., Schröder, C.A., Schneider, A.M., and Behrens, P. (2014). Insight into the mechanism of modulated syntheses: in situ synchrotron diffraction studies on the formation of Zr-fumarate MOF. *CrystEngComm 16*, 9198-9207.

Zhang, G., Meng, F., Guo, Z., Guo, T., Peng, H., Xiao, J., Liu, B., Singh, V., Gui, S., York, P., *et al.* (2018). Enhanced stability of vitamin A palmitate microencapsulated by γ-cyclodextrin metal-organic frameworks. *Journal of Microencapsulation 35*, 249-258.

Zhang, Y.-H., Wang, C.-N., Gong, F.-L., Chen, J.-L., Xie, K.-F., Zhang, H.-L., and Fang, S.-M. (2021). Ultra-sensitive triethylamine sensors based on oxygen vacancy-enriched ZnO/SnO2 micro-camellia. *Journal of Materials Chemistry C 9*, 6078-6086.